Adaptive nonlinear active suspension control based on a robust road classifier with a modified super-twisting algorithm

Yechen Qin, Jagat Jyoti Rath, Chuan Hu, Chouki Sentouh, Rongrong Wang

Nonlinear Dynamics 97/4 (2019) 2425 - 2442

Adaptive nonlinear active suspension control based on a robust road classifier with a modified super-twisting algorithm

Yechen Qin · Jagat Jyoti Rath · Chuan Hu · Chouki Sentouh · Rongrong Wang

Abstract For the suspension system equipped with nonlinear hydraulic actuators and excited by external road conditions, a road adaptive intelligent suspension control strategy is developed. In this work, (1) a multi-phase intelligent road adaptive control architecture is developed to enhance the ride comfort in the presence of varying road excitations; (2) a modified algorithm is proposed to improve the system performance. Initially based on the nonlinear system dynamics, a sliding mode controller based on an improved super-twisting algorithm is proposed. In the Off-line phase, the optimized control parameters based on particle swarm optimization (PSO) approach for each road level are determined and supplied to a probabilistic neural network (PNN)-based classifier for training. In the On-line phase, the PNN classifier employs the measured unsprung mass acceleration to determine the road level and supplies the information to the controller database. Based on the classified road level, corresponding control parameters as determined by PSO are then selected. These control parameters are then supplied to the nonlinear controller which provides the active control. The closed-loop stability of the proposed approach is proved, and the simulation results for different road levels are presented to show the effectiveness of the proposed approach.

Keywords Active suspension control · Nonlinear control · Sliding mode control · Classification · Road adaptive control

Y. Qin
School of Mechanical Engineering, Beijing Institute of Technology, Beijing, People's Republic of China
e-mail: qinyechenbit@gmail.com

J. J. Rath
LAMIH UMR-CNRS 8201, University of Valenciennes, Valenciennes, France

J. J. Rath (✉)
Department of Informatics, Technische Universitat München, Boltzmannstr. 3, 85748 Garching, Germany
e-mail: jagatjyoti.rath@gmail.com

C. Hu
Department of Systems Design Engineering, University of Waterloo, Waterloo, Canada
e-mail: chuan.hu.2013@gmail.com

C. Sentouh
LAMIH UMR-CNRS 8201, Hauts-de-France Polytechnic University, Valenciennes, France
e-mail: chouki.sentouh@univ-valenciennes.fr

R. Wang
School of Mechanical Engineering, Shanghai JiaoTong University, Shanghai, People's Republic of China
e-mail: wrr06fy@gmail.com

1 Introduction

Increasing consumer demand and evolving market trends in recent years have led to the development of road adaptive active suspension systems (ASS), contributing toward improved passenger comfort and

DOI : 10.1007/s11071-019-05138-8

road holding capabilities [1,2]. Typically, the use of hydraulic actuators-based ASS has been widespread in commercial vehicles [3,4] due to their reliability and ease of control capabilities.

The design of commercial ASS controllers has focused in improving the passenger comfort as the vehicle traverses variable road conditions such as bumps, potholes [5] and International Standard Organization (ISO) standard road levels [6] with high velocities. Based on the road and driving conditions, active controllers employing robust strategies have been designed and implemented. Various robust control approaches such as backstepping control [1], sliding mode control [7], H_∞ control [8], fuzzy control [9] and artificial neural network control [10] have been employed to provide active suspension control. In the above works, the robust state feedback controllers were designed to improve the performance of the system considering the road conditions as disturbance to the suspension system. Various works such as [11,12] have employed road profile models based on power spectral density (PSD) analysis for the design of road condition estimators. In contrast, using disturbance observers to estimate road conditions, robust output feedback control approaches for suspension system were proposed in [4,7]. In these works, the observers were designed to estimate road conditions modeled in time–frequency domains [11,12]. Considering practical limitations and cost of sensors, the observers-based road estimation and data-driven road identification approaches offer feasible solutions for the design of adaptive ASSs. However, in comparison with the observer-based techniques [4,13], the data-driven approaches can cater to wider range of road conditions for varying driving scenarios [14–17]. Such data-driven approaches are then used to develop road classifiers/estimators to identify different road conditions. In the works of [13,14], a roughness PSD function based on estimated amplitude was employed for road classification. Based on predefined upper and lower levels of road, thresholds were used to classify the road. Similarly, in [16], the road levels were classified based on time–frequency analysis.

In [18], a road adaptive controller was designed using the information of suspension stoke (i.e., displacement). For this design, the control action switched between soft and stiff suspension behaviors based on the measured stroke. Similarly, in [19,20], the road condition information was employed to switch between active and passive configurations. In [13], a LPV/H-∞ controller was designed to improve passenger comfort of a suspension system using estimated road roughness based on a H-∞ observer. Employing stereo cameras, the road condition information was obtained in [21] and a model predictive control (MPC)-based preview controller was designed to improve the passenger comfort. Considering the works [13,15,18–20], only linear suspension dynamics without any hydraulic actuator were used in the design of controllers. In [13,14], design of road adaptive suspension controllers with variable damping coefficient was discussed for linear suspensions. However, the aspect of active control with nonlinear hydraulic actuators and sensitivity of classification w.r.t. control performance was not discussed. Similarly, closed-loop active nonlinear suspension control was not discussed in [16]. The works proposed in [18,20] considered only bumps, potholes as road disturbances and no random road, i.e., ISO standard roads were considered for analysis.

To address the above issues, we propose a novel road adaptive intelligent suspension control (RAISC) architecture in this paper. For a suspension system equipped with nonlinear hydraulic actuators, a robust higher-order non-singular terminal sliding mode controller (HOSM-NSTSM) using the modified super-twisting approach (STA) is proposed. Accordingly, in this work, (a) a multi-phase road adaptive control architecture is proposed for an active suspension system equipped with nonlinear hydraulic actuators by integrating a PNN-based classifier for road level identification with a robust optimized HOSM-NSTSM controller based on modified STA for active feedback control. (b) Addressing issues of control parameter influence on classifier performance, the closed-loop stability of the adaptive controller is rigorously established by Lyapunov analysis. (c) Performance results of road classification, robustness to parametric uncertainties, sensor noise and comparison with passive suspension, integral HOSM (I-HOSM) [22] control and artificial neural networks (ANN)-based [10] controller are shown for multiple road conditions. Further, extensive discussions on performance of RAISC w.r.t classification interval, selection of superior features and controller performance are also presented. For performance analysis, the proposed control architecture was evaluated for a Class D sedan vehicle equipped with hydraulic actuators over a sequence of three random road levels, i.e., Level A, Level B and Level C.

The rest of this paper is organized as follows. In Sect. 2, the nonlinear active suspension system model and road profile model are described. In Sect. 3, the intelligent classifier and road-aided robust controller are presented. In Sect. 4, simulation results and discussion are carried out to validate the proposed algorithm. The conclusions are presented in Sect. 5.

2 System dynamics

The advent of the independent wheel configurations in modern commercial automobiles [6] focuses on the design of controllers specific to a quarter wheel configuration. Under the assumptions that roll and pitch motions of the vehicle are negligible, the active suspension control problem for a quarter wheel vehicle is formulated and the classifier-based control design is discussed consequently. For the quarter wheel configuration, motion is regulated by the dynamics of wheel hop, vehicle chassis and the road–wheel interactions, as shown in Fig. 1. To provide active suspension control, hydraulic actuators [1,23] have been employed in the commercial vehicles [3,4] and considered in this paper.

The governing dynamics for the sprung and unsprung masses can be given as [6,7]:

$$\begin{cases} m_b\ddot{x}_b = -F_\mathrm{s} - c_\mathrm{p}(\dot{x}_b - \dot{x}_w) + F_a, \\ m_w\ddot{x}_w = F_\mathrm{s} - k_\mathrm{t}(x_w - x_f) + c_\mathrm{p}(\dot{x}_b - \dot{x}_w) - F_a, \end{cases} \tag{1}$$

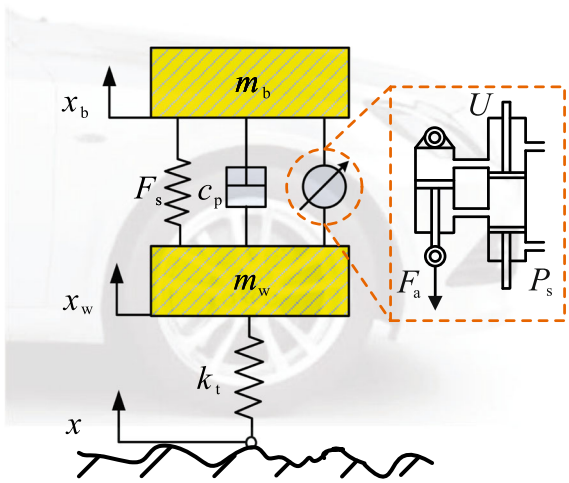

Fig. 1 Two-degree-of-freedom model of the active suspension system

where m_b, m_w denote the sprung and unsprung masses, respectively, x_b, x_w represent the sprung and unsprung mass vertical displacements, x_f is the external input from road, F_a is the active force generated by the hydraulic actuator, F_s is the nonlinear spring force and c_p, k_t denote the suspension damping and tire stiffness coefficients, respectively. The nonlinear spring force is modeled as:

$$\begin{cases} F_\mathrm{s} = k_\mathrm{s}\,(x_b - x_w) + \varphi_a, \\ \varphi_a = k_n(x_b - x_w)^3, \end{cases} \tag{2}$$

where k_s is the spring stiffness and φ_a denotes the nonlinear component, with k_n representing the nonlinear spring force [4]. The effect of the road excitation on the suspension system is represented by the external disturbance x_f acting as dynamic vertical tire load.

Under the assumption that road profile is a homogeneous and isotropic Gaussian random process [11], the dynamic model of road excitation can be written as:

$$G_q(n_\mathrm{s}) = G_q(n_o)\left(\frac{n_\mathrm{s}}{n_o}\right)^{-W}, \tag{3}$$

where $G_q(n_\mathrm{s})$ is the PSD of the road excitation, n_s is the spatial frequency, $G_q(n_o)$ represents the excitation energy and $W = 2$ represents the road structure as per ISO-8608 [11]. Consequently, based on the PSD values, various levels of roads, i.e., Level A–Level H, can be modeled as per the harmony function superposition method [24], which approximates the road PSD with a series of harmonic functions. For a given frequency range $[f_1, f_2]$, we can equally divide it into M parts. The middle frequency $f_{\mathrm{mid}-K}$ is then taken to replace the Kth $(K = 1, 2, \ldots M)$ frequency range. According to the Plancherel theorem, the integral of a function's squared modulus is equal to the integral of the squared modulus of its frequency spectrum. Therefore, the amplitude of Kth part can be written as:

$$A_K = \sqrt{G_q\,(f_{\mathrm{mid}-K}) \cdot \Delta f_K}. \tag{4}$$

By summing M sine functions with frequency and amplitude defined by $f_{\mathrm{mid}-K}$ and (5), respectively, the generated road profile can be analytically expressed as:

$$q\,(t) = \sum_{K=1}^{M} \sqrt{2 \cdot G_q\,(f_{\mathrm{mid}-K}) \cdot \frac{f_2 - f_1}{M}} \sin\left(2\pi\, f_{\mathrm{mid}-K}\, t + \Phi_K\right), \tag{5}$$

where Φ_K is an independent and identically distributed random phase shift in the range $(0, 2\pi)$.

The active force F_a is generated by a four valve hydraulic actuator based on the control input which is generally a current/voltage signal. The control force, F_{a}, can be obtained as $F_{\mathrm{a}} = P_L A_{\mathrm{p}}$, where the valve piston area is A_{p} and the pressure drop across the piston is denoted as P_L. The dynamics of the P_L is given as [1,25]:

$$\dot{P}_L = \lambda_1(P_{\mathrm{s}}, P_L)U - C_{\mathrm{tp}}\alpha P_L - A_{\mathrm{p}}^2\alpha(\dot{x}_b - \dot{x}_w), \quad (6)$$

where $\alpha = \frac{4\beta_e}{V_{\mathrm{t}}}$, U is the control current/voltage, V_{t} is the actuator volume, β_{e} is the effective bulk modulus, C_{tp} is the total piston leakage coefficient, λ_1 is the load flow, which can be expressed as:

$$\lambda_1 = \frac{A_{\mathrm{p}}C_{\mathrm{d}}\omega\alpha}{\sqrt{\rho}}\sqrt{\left|P_{\mathrm{s}} - \frac{\mathrm{sign}(U)P_L}{A_p}\right|}, \quad (7)$$

where C_{d} is the discharge coefficient, ω is the spool valve area gradient, ρ is the fluid density and P_{s} is the supply pressure.

Integrating the above dynamics, a nonlinear state space model can be formulated with the states as:

$$x = \begin{bmatrix} x_1 & x_2 & x_3 \end{bmatrix}^T = \begin{bmatrix} x_b - x_w & \dot{x}_b - \dot{x}_w & MF_a \end{bmatrix}^T.$$

The state dynamics can then be expressed as:

$$\begin{cases} \dot{x}_1 = x_2, \\ \dot{x}_2 = x_3 + \varphi_1(x,t) + f_u(t), \\ \dot{x}_3 = \lambda_u(x,t)U + \varphi_2(x,t), \end{cases} \quad (8)$$

where

$$\begin{aligned} \lambda_u &= \frac{A_{\mathrm{p}}C_{\mathrm{d}}\omega\alpha}{\sqrt{\rho}}\sqrt{\left|P_{\mathrm{s}} - \frac{\mathrm{sign}(U)x_3}{MA_{\mathrm{p}}}\right|}, \\ \varphi_1 &= -M\varphi_a - k_{\mathrm{s}}Mx_1 - c_{\mathrm{p}}Mx_2, \\ \varphi_2 &= -\lambda_2 x_3 - M\lambda_3 x_2, \\ \lambda_2 &= C_{\mathrm{tp}}\alpha,\ \lambda_3 = A_{\mathrm{p}}^2\alpha, \\ M &= \frac{m_b + m_w}{m_b m_w},\ f_u = \frac{k_{\mathrm{t}}(x_w - x_r)}{m_w}. \end{aligned} \quad (9)$$

The design of the active suspension control is a multi-objective task [6] where the contradicting aspects of the stability and the comfort must be accounted for. The performance of any active suspension controller in terms of the passenger comfort enhancement can be measured by the reduction in the sprung mass acceleration, $\ddot{x}_b$. Similarly, the stability of vehicle, i.e., its capability to stay on the road, is measured by the tire deflection, i.e., $T_{\mathrm{def}} = (x_w - x_f)$. It is of note that typically based on the control objective, either the road holding or passenger comfort can be considered as a constraint for ease of design [1,4,6]. On similar lines, a multi-phase intelligent road adaptive control architecture is proposed to improve the vehicle ride comfort, while considering road holding as a necessary constraint to be satisfied. Based on road holding, mechanical design and actuator limits, the following constraints for the controller design are considered:

1. The suspension stroke $x_b - x_w$ is constrained by ± 0.08 m.
2. The maximum force F_a generated by the hydraulic actuator is constrained by ± 1500 N.
3. The road holding ability is defined by $S_{\mathrm{c}} = \frac{F_{\mathrm{dyn}}}{F_{\mathrm{st}}} < 1$, where $F_{\mathrm{dyn}} = k_{\mathrm{t}}(x_w - x_f)$ is the dynamic vertical tire load and $F_{\mathrm{st}} = (m_w + m_b)g$ is the static vertical tire load.

3 Intelligent classifier and robust controller

The control objective for the proposed work is to improve passenger comfort while considering safety constraints such as road holding, suspension stroke and actuator limitations. To achieve this, we propose a multi-phase design where a robust HOSM-based nonlinear control law is used in conjunction with a PNN-based road classifier. The architecture of the proposed approach is first discussed followed by the design of controller, classifier and classifier-based control subsequently.

3.1 Proposed architecture

The design of the proposed RAISC for the suspension system integrates a robust HOSM-NSTSM-based nonlinear feedback robust control with a PNN-based road level classifier. Based on classified road level information, optimized control parameters are used to provide effective control in real time. To realize this, the architecture is developed over two phases, i.e., (1) Off-line phase for training of classifier and (2) On-line phase for classifier validation and controller action with the controller database interlinking these phases as shown in Fig. 2.

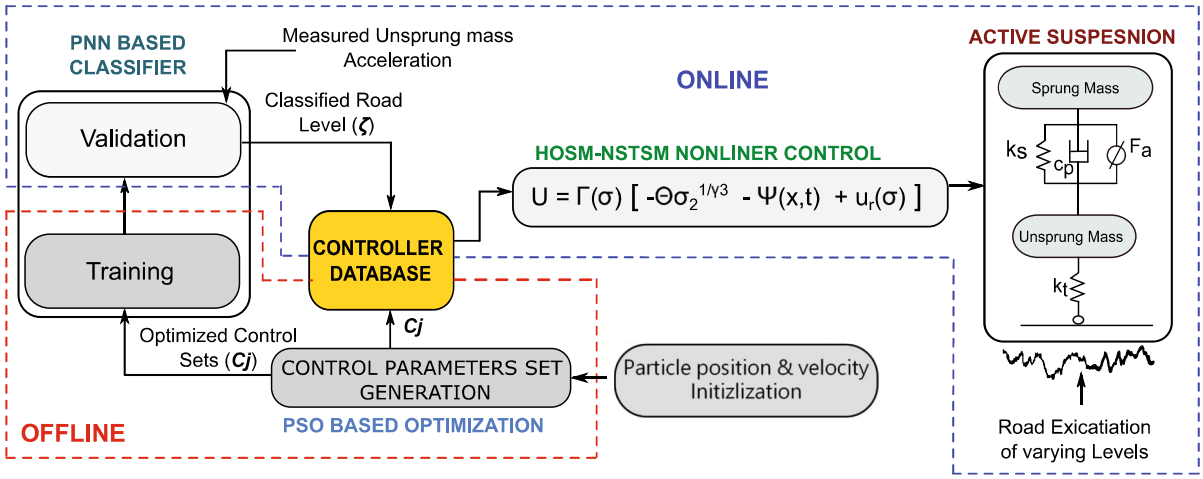

Fig. 2 Architecture of the proposed RAISC scheme

The Off-line phase of operation consists of two modules—(i) control parameters set generation module (ii) training of the PNN-based classifier. Based on the control law to be discussed later, first a set of control parameters C_j is determined. Accordingly, in control parameter set generation module, PSO is employed to generate the optimal control parameter sets corresponding to individual road levels. These optimal control parameter sets C_j are then stored in the controller database unit and also provided to the training phase of the PNN classifier. Subsequently, the PNN classifier then selects the insensitive frequency ranges w.r.t the optimized control parameter sets. Based on the extracted features, the classifier is trained and the information provided to the classifier validation stage of the On-line phase. In the On-line phase, the operation is categorized into (i) validation of the PNN classifier followed by road level identification and (ii) robust HOSM-NSTSM control action generation for the suspension system. Based on real-time excitation of the suspension for various road conditions, the unsprung mass acceleration is measured. After sampling of this signal at a rate of 100 Hz, it is fed to the PNN classifier in real time. Based on the information from the Off-line classifier training module and the sampled unsprung mass acceleration signal, the classification validation module generates the information of road level ζ which is supplied to the controller database. Using this information of road level, the optimal control parameters set C_j which were obtained previously during the Off-line phase are directly selected from the controller database and provided to the controller in real time. Thus, the controller database unit acts as a lookup table from which optimal control parameters generated in the Off-line phase can be directly selected in the On-line phase. The use of control database unit prevents any unwarranted switching between the Off-line and On-line phase and simplifies the design.

3.2 Robust HOSM-NSTSM controller design

In this section, we discuss the design of the robust higher-order non-singular terminal sliding mode controller (HOSM-NSTSM) for the nonlinear active suspension system (8) based on state feedback. Sliding mode controller is widely applied for vehicle dynamics control [26,27]. To design the active control U, a recursive structure similar to [28] is followed, avoiding the singularity in the design. In [28], a first-order sliding mode term is employed for disturbance rejection and subsequent approximations of the discontinuous term are done for design. Improving on the work of [28], we discuss the design of a recursive NSTSM controller employing a HOSM-based modified super-twisting algorithm (STA) in this section. The control problem is thus formulated as tracking the reference x_{d} for the suspension stroke. Further, as the relative degree of control input U w.r.t to the state x_1 is 3, two recursive terminal error surfaces can be designed as:

$$\begin{cases} \sigma_0 = x_1 - x_{\mathrm{d}}, \\ \sigma_1 = \beta_1 \sigma_0 + \dot{\sigma}_0^{\gamma_1}, \\ \sigma_2 = \beta_2 \sigma_1 + \dot{\sigma}_1^{\gamma_2}, \end{cases} \tag{10}$$

where $\beta_1, \beta_2 > 0$ are positive constants to be designed. For the designed error surfaces, the parameters $\gamma_i, i = 1, 2, 3$ are designed as a ratio of two odd integers, i.e., $\gamma_i = p_i/q_i$, with the integers $p_i > q_i > 0$ chosen to ensure a non-singular design. An integral non-singular terminal sliding surface which depends on the recursive error surfaces σ_i is designed as:

$$S = \sigma_2 + \Theta \int_0^t \sigma_2^{\frac{1}{\gamma_3}} \, \mathrm{d}t, \tag{11}$$

where $\Theta > 0$ and γ_3 is designed similar to γ_1, γ_2. It is of note that the selection of coefficients γ_i must obey the condition, $\gamma_i > 3 - i$ similar to [28]. Substituting for the dynamics of the error surfaces σ_2, σ_1 and σ_0, the sliding surface dynamics from (11) can be written as:

$$\dot{S} = \Theta \sigma_2^{\frac{1}{\gamma_3}} + \beta_1\beta_2\dot{\sigma}_0 + f_1(x)\ddot{\sigma}_0 + f_2(x)\ddot{\sigma}_0^2 + f_3(x)\dddot{\sigma}_0, \tag{12}$$

where

$$\begin{cases} f_1(x) = \beta_2\gamma_1\dot{\sigma}_0^{\gamma_1 - 1} + \beta_1\gamma_2\dot{\sigma}_1^{\gamma_2 - 1}, \\ f_2(x) = \gamma_1\gamma_2\dot{\sigma}_1^{\gamma_2 - 1}\dot{\sigma}_0^{\gamma_1 - 2}, \\ f_3(x) = \gamma_1\gamma_2\dot{\sigma}_1^{\gamma_2 - 1}\dot{\sigma}_0^{\gamma_1 - 1}. \end{cases} \tag{13}$$

The successive derivatives of the error surface σ_0 can then be given as:

$$\begin{cases} \dot{\sigma}_0 = x_2 - \dot{x}_\mathrm{d}, \\ \ddot{\sigma}_0 = x_3 + \varphi_1 + f_u - \ddot{x}_\mathrm{d}, \\ \dddot{\sigma}_0 = M\lambda_u U + \varphi_2 - \dddot{x}_\mathrm{d} + \dot{\varphi}_1 + \dot{f}_u. \end{cases} \tag{14}$$

Substituting with the dynamics of σ_0 in (10), (12) can be then written as:

$$\dot{S} = \Theta\sigma_2^{\frac{1}{\gamma_3}} + \Psi(x,t) + f_3(x)M\lambda_u U + \Delta, \tag{15}$$

where Δ is the disturbance, which can be described as:

$$\Delta = f_1(x)f_u + f_2(x)f_u^2 + f_3(x)\dot{f}_u, \tag{16}$$

The nonlinear function $\Psi(x,t)$ can be calculated as:

$$\begin{aligned} \Psi(x,t) = {} & \beta_1\beta_2 g_1(x,t) + f_1(x)g_2(x,t) \\ & + f_2(x)g_2(x,t)^2 + f_3(x)g_3(x,t), \end{aligned} \tag{17}$$

where $g_1(x,t) = x_2 - \dot{x}_\mathrm{d}$, $g_2(x,t) = x_3 + \varphi_1 - \ddot{x}_\mathrm{d}$, $g_3(x,t) = \varphi_2 - \dddot{x}_\mathrm{d} + \dot{\varphi}_1$. To ensure the convergence of the sliding dynamics $S = 0$, in the presence of the lumped disturbance term Δ, the feedback control U will be presented.

The following lemmas are essential for the proof of the consequent theorem [29,30].

Lemma 1 *Assume $z_1(t)$ and $z_2(t)$ are two locally absolute continuous functions, then the function:*

$$V(t) = \zeta^T P\zeta, \tag{18}$$

is locally absolute continuous, where $P \in \Re^{2\times 2}$ is a p.d. matrix, where $\zeta = \left[\, |z_1|^\beta sign(z_1)\ z_2 \,\right]^T$ and $1 > \beta > 0.5$.

Lemma 2 *If a function $V(t)$ is absolute continuous on some interval, then $V(t)$ is monotonously decreasing if and only if $\dot{V}$ is negative definite everywhere.*

Theorem 1 *For the considered active suspension system with the sliding dynamics (15), the following control is proposed:*

$$U = \Gamma(x)\left[-\Theta\sigma_2^{\frac{1}{\gamma_3}} - \Psi(x,t) + u_\mathrm{r}(S)\right], \tag{19}$$

where $\Gamma(x) = \frac{1}{f_3(x)M\lambda_u}$ and the robust higher-order sliding mode (HOSM)-based robust control $u_\mathrm{r}(S)$ is given as:

$$u_\mathrm{r}(S) = -\kappa_1|S|^\beta \mathrm{sign}(S) - \kappa_2\int_0^t |S|^\theta \mathrm{sign}(S)\,\mathrm{d}t, \tag{20}$$

where $1 - 2\beta + \theta = 0$ and $1 > \beta \geq 0.5$. $\kappa_1, \kappa_2 > 0$ are the positive gains to be designed. Employing the nonlinear state feedback control (19), the sliding surface attains the practical bounded stability around the equilibrium in finite time.

Proof Considering the sliding dynamics (15) and substituting the control U, the derivate of S can be written as:

$$\begin{aligned} \dot{S} = {} & f_3(x)M\lambda_u\Gamma(x)\left[-\Theta\sigma_2^{\frac{1}{\gamma_3}} - \Psi(x,t) + u_\mathrm{r}(S)\right] \\ & + \Theta\sigma_2^{\frac{1}{\gamma_3}} + \Psi(x,t) + \Delta. \end{aligned} \tag{21}$$

The convergence of the sliding dynamics employing the feedback control U is dependent on the nonsingularity of the function $f_3(x)$ which affects the term $\Gamma(x)$. To avoid singularity, the following condition is invoked for $f_3(x)$:

$$\Omega \equiv \begin{cases} \prod_{j=1}^{2} \dot{\sigma}_{j-1}^{\gamma_j - 1}, & \text{for} \quad \left| \prod_{j=1}^{2} \dot{\sigma}_{j-1}^{\gamma_j - 1} \right| \geq \epsilon \\ \epsilon & \text{otherwise} \end{cases} \tag{22}$$

for $j = 1, 2$ and $\epsilon > 0$ is a positive constant. The above expression can be understood as a saturated scenario for the nonlinear function $f_3(x)$. It can be deduced from the above expression that now two scenarios arise depending on the magnitude of the error surfaces σ_0 and σ_1. In the first scenario when $\left| \prod_{j=1}^{2} \dot{\sigma}_{j-1}^{\gamma_j - 1} \right| \geq \epsilon$, the nonlinear function $f_3(x)$ is not approximated and invertible, which can avoid the singularity in control design. Thus, the sliding dynamics in such a case can be expressed as:

$$\dot{S} = u_{\mathrm{r}}(S) + \Delta. \tag{23}$$

The disturbance term Δ is a function of the nonlinear terms $f_1(x)$, $f_2(x)$, $f_3(x)$ and the road perturbation f_u. The nonlinear terms are the functions of the error surfaces σ_0, σ_1 and their first-order derivatives. As discussed in the singularity clause for the design of the error functions, it can be ensured that both $\dot{\sigma}_0$ and $\dot{\sigma}_1$ are differentiable. Further, for all practical purposes, the road disturbance f_u and its successive derivatives are bounded. Consequently, with the assumptions on the boundedness of the road disturbance f_u, the bound of the perturbation Δ can be established as $|\dot{\Delta}| < \delta$, for $\delta > 0$ being a positive bound.

Define

$$\begin{aligned} \eta &= -\kappa_2 \int_0^t |S|^{\theta} \operatorname{sign}(S)\, \mathrm{d}t + \Delta, \\ \zeta &= \left[|S|^{\beta} \operatorname{sign}(S) \;\; \eta \right]^T. \end{aligned} \tag{24}$$

Then, the derivate of ζ can be calculated as:

$$\dot{\zeta} = \frac{1}{|S|^{1-\beta}} A\zeta + \left[0 \;\; 1 \right]^T \dot{\Delta}. \tag{25}$$

where

$$\begin{aligned} A &= \begin{bmatrix} -\beta\kappa_1 & \beta \\ -\kappa_2 |S|^{\theta+1-2\beta} & 0 \end{bmatrix} \\ &= \begin{bmatrix} -\beta\kappa_1 & \beta \\ -\kappa_2 & 0 \end{bmatrix}. \end{aligned}$$

Since $\beta, \kappa_1, \kappa_2 > 0$, all the eigenvalues of A locate in the negative real part. Then, the p.d. matrix P can be chosen as:

$$PA + A^T P = -Q < 0. \tag{26}$$

The candidate Lyapunov function is chosen as:

$$V = \zeta^T P \zeta. \tag{27}$$

With $e_2 = \left[0 \;\; 1 \right]^T$, the derivate of (27) is calculated as:

$$\begin{aligned} \dot{V} &= -\frac{1}{|S|^{1-\beta}} \zeta^T Q \zeta + 2\zeta^T P e_2 \dot{\Delta} \\ &\leq -\frac{1}{|S|^{1-\beta}} \zeta^T Q \zeta + 2 \left| \zeta^T P e_2 \right| \delta \\ &\leq -\frac{1}{|S|^{1-\beta}} \zeta^T Q \zeta + \frac{1}{\omega} \|S\| \delta + \omega e_2^T P^T P e_2 \delta, \end{aligned} \tag{28}$$

where ω is a positive number. Let $\omega = |\zeta|^{1-\beta}/\mu$, (28) can be calculated as:

$$\begin{aligned} \dot{V} &\leq -\frac{1}{|S|^{1-\beta}} \zeta^T (Q - \mu\delta I) \zeta + \frac{|S|^{1-\beta}}{\mu} e_2^T P^T P e_2 \delta \\ &\leq -\lambda_{\min}(Q - \mu\delta I) \frac{\|\zeta\|^2}{|S|^{1-\beta}} + \frac{|S|^{1-\beta}}{\mu} e_2^T P^T P e_2 \delta. \end{aligned} \tag{29}$$

Considering that

$$\begin{aligned} &|S|^{\beta} \leq \|\zeta\|, \\ &\lambda_{\min}(P) \|\zeta\|^2 \leq V \leq \lambda_{\max}(P) \|\zeta\|^2, \end{aligned}$$

(29) can be calculated as:

$$\begin{aligned}\dot{V} &\leq -\lambda_{\min}(Q-\mu\delta I)\frac{\|\zeta\|^2}{|\zeta|^{\frac{1-\beta}{\beta}}}+\frac{|\zeta|^{\frac{1-\beta}{\beta}}}{\mu}e_2^T P^T P e_2\delta \\ &= -\lambda_{\min}(Q-\mu\delta I)\|\zeta\|^{3-\frac{1}{\beta}}+\frac{\|\zeta\|^{\frac{1}{\beta}-1}}{\mu}e_2^T P^T P e_2\delta \\ &\leq -\lambda_{\min}(Q-\mu\delta I)\left(\frac{V}{\lambda_{\max}(P)}\right)^{\frac{3\beta-1}{2\beta}} \\ &\quad+\left(\frac{V}{\lambda_{\max}(P)}\right)^{\frac{1-\beta}{2\beta}}\frac{1}{\mu}e_2^T P^T P e_2\delta.\end{aligned} \tag{30}$$

Denote

$$\begin{cases} z=\dfrac{V}{\lambda_{\max}(P)}, \\ g_1=\dfrac{3\beta-1}{2\beta}, g_2=\dfrac{1-\beta}{2\beta}, \\ k_1=-\lambda_{\min}(Q-\mu\delta I), \\ k_2=\dfrac{1}{\mu}e_2^T P^T P e_2\delta. \end{cases} \tag{31}$$

Define an auxiliary variable as:

$$\tilde{z}=\frac{1}{1-g_2}z^{1-g_2}.$$

When $z>0$, the derivative of $\tilde{z}$ can be calculated as:

$$\begin{aligned}\dot{\tilde{z}} &= z^{-g_2}\dot{z} \\ &= -k_1 x^{g_1-g_2}+k_2 \\ &= -k_1(1-g_2)^{\frac{g_1-g_2}{1-g_2}}\tilde{z}^{\frac{g_1-g_2}{1-g_2}}+k_2.\end{aligned} \tag{32}$$

Define

$$V_1=|\tilde{z}|^{\frac{g_1-g_2}{1-g_2}+1},$$

and if

$$|\tilde{z}|>\frac{1}{1-g_2}\left(\frac{k_2}{k_1}\right)^{\frac{1-g_2}{g_1-g_2}}.$$

Then, it is not difficult to derive $\dot{V}_1<0$. Hence, one can conclude that

$$\lim_{t\to\infty}\sup|\tilde{z}|\leq\frac{1}{1-g_2}\left(\frac{k_2}{k_1}\right)^{\frac{1-g_2}{g_1-g_2}}. \tag{33}$$

According to (33), the supremum of V can be calculated as:

$$\lim_{t\to\infty}\sup V\leq\left(\frac{e_2^T P^T P e_2\delta\lambda_{\max}(P)^{\frac{2\beta-1}{2\beta}}}{\mu\lambda_{\min}(Q-\mu\delta I)}\right)^{\frac{\beta}{2\beta-1}}.$$

Further, by considering

$$|S|\leq\|\zeta\|^{\frac{1}{\beta}}\leq\left(\frac{V}{\lambda_{\min}(P)}\right)^{\frac{1}{2\beta}},$$

The supremum of S is given as:

$$\begin{aligned}&\lim_{t\to\infty}\sup|S| \\ &\leq\left(\frac{\sqrt{\lambda_{\max}(P)}}{\lambda_{\min}}\right)^{\frac{1}{2\beta}}\left(\frac{e_2^T P^T P e_2\delta}{\mu\lambda_{\min}(Q-\mu\delta I)}\right)^{\frac{1}{2(2\beta-1)}}.\end{aligned}$$

In the second scenario, when $\left|\prod_{j=1}^{2}\dot{\sigma}_{j-1}^{\gamma_j-1}\right|<\epsilon$, the saturated value of $f_3(x)$, i.e., ϵ is considered in the design ensuring that there is no singularity. In such a scenario, the sliding surface can be approximated as:

$$\left|\dot{S}\right|\leq f(x,\delta,\nu)=\bar{\nu}_2.$$

The convergence of the sliding surface S to a finite bound around the origin can be established. It is of note that the perturbation affecting the system is nonvanishing and hence the sliding surface attains only practical convergence, i.e., convergence to a finite bound. The magnitude of this bound is dependent on the value of ϵ discussed earlier. □

To ensure robust and optimal performance of the proposed HOSM-NSTSM controller for each road level, the gains of the controller are optimized using PSO technique in the Off-line phase. The results of the PSO-based optimization for each controller are stored as an optimal control parameter set in the controller database block as shown in Fig. 2. In this work, the focus was on optimizing the robust control performance and subsequently based on the chosen values of Θ and γ_i such that the singularity condition is avoided, and the optimal control parameter sets are formulated as

$$C_j=\left[\kappa_{1j}\ \kappa_{2j}\ \beta_{1j}\ \beta_{2j}\right], \tag{34}$$

DOI : 10.1007/s11071-019-05138-8

where $j = A, B, C$ signifies the individual controllers, i.e., Controller A, Controller B and Controller C. With the nonlinear controller designed, we now discuss the intelligent classifier which generates the information of the road level on basis of which the controller database block decided the appropriate control parameter set.

Remark 1 Considering the function λ_u can be written as:

$$\lambda_u = \frac{A_p C_d \omega \alpha}{\sqrt{\rho}} \sqrt{|P_s - \frac{\text{sign}(U)x_3}{MA_p}|}, \tag{35}$$

where P_s is the supply pressure of the fluid, A_p is the piston area, C_d is the discharge coefficient, ω is the valve width, α is a function of bulk modulus of fluid and U is the control input. It can be seen that the function λ_u is non-singular at all times except when $P_s = \frac{\text{sign}(U)x_3}{MA_p}$, i.e., when supply pressure is equivalent to the pressure difference across the valves. However, for physical operating conditions of the hydraulic actuator, the pressure difference across the valves does not increase the supply pressure [25]. Thus, the function λ_u does not lead to a singularity in design as required for the convergence of the sliding dynamics.

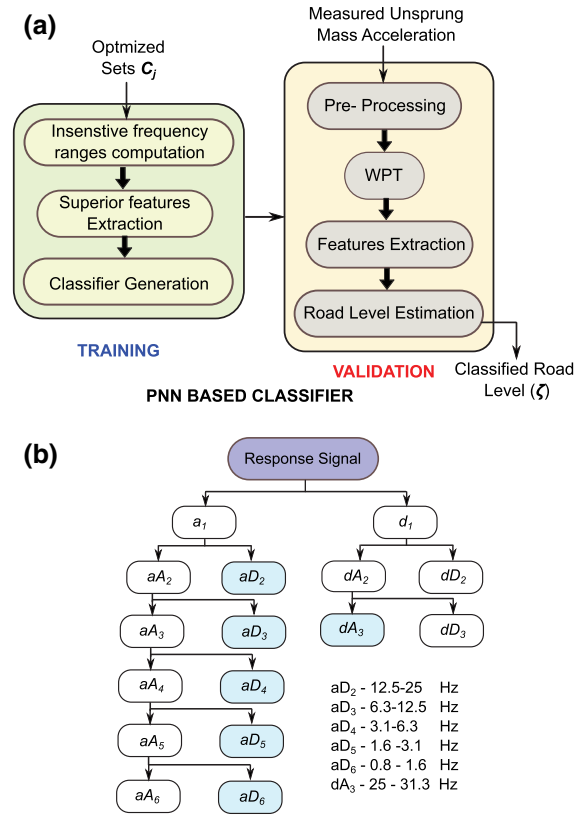

Fig. 3 **a** Proposed PNN-based classifier. **b** Six-layer structure of WPT

3.3 Intelligent classifier design

To ensure high performance of the proposed RAISC scheme, a PNN-based road classification technique that is robust to the optimized controller parameter C_j variations is proposed in this work as shown in Fig. 3a. It should be noted that in [13,14], a roughness PSD function based on estimated amplitude was employed for road classification with predefined upper and lower levels of road for threshold selection. For the design of RAISC, we propose to use twelve statistical features, employ mRMR for superior feature selection and then train a PNN-based classifier to find the superior features. Subsequently, the classifier then identifies the roads without the use of any predefined thresholds. The road classification method is developed based on the time–frequency analysis techniques similar to the work proposed in [16]. The sequential development of the intelligent classifier is detailed as follows:

Step 1: Selection of insensitive frequency ranges

In this work, the concept of signal sensitivity analysis on basis of which insensitive frequency ranges are determined is proposed. The objectives of introducing this procedure and hence the insensitive frequency range selection were: (a) to determine which system response (i.e., sprung mass/unsprung mass acceleration) is best suited for the classification of road level (b) to ensure that the selected system response is invariant to the effect of control parameter sets C_j.

To find the insensitive frequency ranges, frequency characteristics curves for the measured system responses are firstly computed. The road input for various levels of roads (3) has random nature; hence, the generated frequency curves show high fluctuations in the high-frequency range. A series of excitations Λ_p are considered to decompose the standard road profiles

defined by ISO-8608 into numbers of sine functions and given as:

$$\Lambda_p = \sqrt{2G_q(f_p)}(2\pi f_p t), \tag{36}$$

where the frequency range (0.33–28.3 Hz) into P parts with f_p defined as the pth middle frequency and $G_q(f_p)$ is the PSD of f_p. For time–frequency analysis, a six-layer wavelet packet transformation (WPT) is performed to partition the frequency characteristics curve into six components as shown in Fig. 3b. In this paper, a frequency range of 0.33–28.3 Hz has been considered for analysis purposes. Owing to the down-sampling of the WPT, an approximated range of 0.8–31.3 Hz has been adapted as shown in the various frequency components in Fig. 3b. In order to select the insensitive frequency range based on the system response of each controller parameter set, the following *insensitive index* which depicts the incidence of individual frequency range caused by different controller parameter sets C_j is proposed as follows:

$$\theta_\eta = \left| 1 - \Sigma_{i=1,3} w_i \left(\frac{\Sigma_{d_\eta}^{g_\eta} \Gamma_i(f_p)}{\Sigma_{d_\eta}^{g_\eta} \Gamma_2(f_p)} \right) \right| \forall \eta = 1, \ldots, 6, \tag{37}$$

where η represents the ηth frequency component generated by the WPT, g_η, d_η are the upper and lower frequency limits of η, w_i is the weighting factor and $\Gamma_i(f_p)$ is the RMS (root mean square) of the system response generated under action of the typical controller parameter set C_j with the excitation frequency f_p. In this paper, it is considered that all controller parameters have the equal importance and subsequently $w_i = 0.5, i = 1, 3$ are chosen. The obtained *insensitive index* θ_η is then sorted in the ascending order, and the first three indexes with the lowest values are denoted as Ω_1, Ω_2 and Ω_3, respectively.

Further, to ensure that proper information is available for the classification, the following constraint is defined:

$$\frac{d_\eta}{\lambda} \geq 3\,\mathrm{s}^{-2}, \tag{38}$$

where λ is the classification interval and d_η is the lower frequency bound discussed in (37). The necessity of the constraint (38) is justified: (a) to ensure a limited effect of the reduction in information in (37) as a result of fewer availability of PSD points in low-frequency ranges. This typically occurs due to the use of constant bandwidth PSD computation method (b) to limit the existing bias of the sampled signal which influences the classification accuracy significantly. Satisfying the constraint (38) thus ensures that sufficient information is available for classification of road level during Online phase of operation. It should be noted that Ω_1, Ω_2 and Ω_3 obtained from (37) are used to determine the applicable system response. For robustness, a variable γ is then defined as

$$\gamma = \frac{\Omega_1 + \Omega_2 + \Omega_3}{3}. \tag{39}$$

The response with the smallest γ is then used as the only measured signal for the road classification.

Step 2: Extraction of superior features

After selection of the insensitive frequency ranges, the statistical features of both time and frequency domains are calculated according to the basic features set and the superior features are then selected by a feature selection method. Based on previous studies for road excitation classification [16], variance (VAR), square root of amplitude (SRA) and RMS were established as the most suitable statistical features. With the basic features established, the statistical features' database for the selected *insensitive frequency* ranges Ω_1, Ω_2, Ω_3 and in time domain is shown in Table 1 with Ψ_ν, $\nu = 1, \ldots, 12$ representing the features index. Although all 12 features can be used as the input of the classifier, they are not of the same importance and there exists data redundancy [16]. Thus, maximal relevance and minimum mutual redundancy (mRMR) method is employed in this paper for the feature selection [16].

Table 1 Statistical features indexes

Domain	Features	(VAR)	(SRA)	(RMS)
Time domain		1	2	3
Frequency domain	Ω_1	4	5	6
	Ω_2	7	8	9
	Ω_3	10	11	12

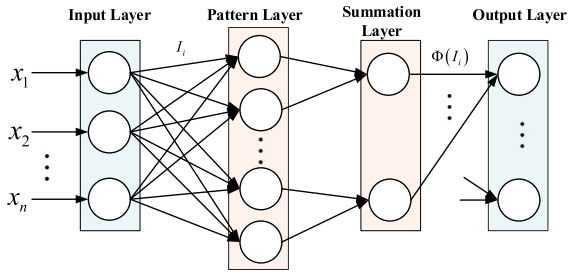

Fig. 4 Structure of the PNN

Step 3: Generation of classifier and validation

The computed superior features in STEP 2 are then fed to a classifier which then outputs excitation level accordingly. Based on the appropriate chosen training and testing data sets, the classifier then provides the information of the estimated road excitation. It is of note that to improve signal quality and classification accuracy, low-pass filtering and framing are employed as the signal preprocessing techniques. In this paper, based on the predefined features and categories, PNN [31] uses a training set to develop a distribution function to calculate the likelihood of features within different categories as shown in Fig. 4, and the structure of the PNN-based classifier is shown in Fig. 3a.

The weighted sum of each neuron is calculated as per a nonlinear activation function:

$$\Phi\left(I_i\right) = \mathrm{e}^{\frac{I_i - 1}{\sigma^2}}, \tag{40}$$

where I_i is the ith weight between the input and the pattern layer, and σ is a smoothing factor.

Then, a final output is obtained which indicates the typical road level ζ, i.e., Road Level A, B or C, respectively, as shown in Fig. 3a in the On-line phase of operation. For further details, refer [31]. This output of the classifier is then provided to the controller database block in the On-line stage as discussed earlier.

Remark 2 In this work, mRMR and PNN are utilized for feature selection and classifier generation, respectively. It is of note that there are various other approaches such as improved distance evaluation method [17] and adaptive neuro-fuzzy inference system (ANFIS) [17] which can be employed to solve the above problem. In this work, these two techniques are employed to illustrate the feasibility of the proposed method and can be replaced by the other methods described above based on design.

3.4 Classification-aided controller RAISC

The controller database block forms the link between the Off-line and the On-line phases, acting as a decision module which generates the controller parameters specific to the typical road excitation level. It should be noted that there is no switching between the On-line and Off-line phase to obtain control parameters. Based on the road level ζ information obtained from the PNN-based classifier, a simple switching rule is then employed to select the appropriate controller control parameter C_j set in the controller database block. The switching only occurs in the On-line phase when different road levels are detected. Thus, if the road level switches form Level A to Level B, the typical control parameters are selected from the controller database. This entire operation occurs in the On-line phase and is supplemented by that fact that the controller database is the only unit which is part of the Off-line and On-line phases as shown in Fig. 2. With the controller parameter set identified, the proposed control law (19) ensures the convergence of the sliding surface in finite time as discussed in Theorem 1. The convergence of the sliding surfaces ensures robust closed-loop state feedback operation and hence improvement in the passenger comfort. In contrast to the previous approaches [19], in this work the classifier proposed is insensitive to the PSO-based optimized control gains. Further, the influence of classification interval and selection of superior features is considered such that accurate information of the road level is obtained. Thus, in the case of various road levels the closed-loop robust performance of the controller can be established.

4 Simulation results and discussion

In this section, the evaluation of the proposed adaptive control scheme for three levels of roads, i.e., Level A, Level B and Level C, is presented. The selection of optimal control gains based on PSO technique for controllers for each road class, the classifier to estimate the road excitation and the adaptive controller based on the classifier information is subsequently discussed.

4.1 Parameter selection

The evaluation of the proposed RAISC scheme was performed on the signal responses obtained by the sim-

ulation of suspension dynamics of a Class D sedan. For the considered vehicle, the system parameters for the quarter car dynamics (1) were chosen as [4] sprung mass $m_b = 342.5$ kg, unsprung mass $m_w = 40$ kg, tire stiffness $k_t = 268{,}000$ Nm, suspension spring stiffness $k_s = 18{,}000$ Nm, suspension damping coefficient $c_p = 1000$ Ns/m, supply pressure $P_s = 1.034 \times 10^7$ Pa, piston area $A_p = 3.35 \times 10^{-4}$ m^2, $\alpha = 4.515 \times 10^{15}$ N/m^5, spool valve area $\omega = 1.436 \times 10^{-2}$ m^2, discharge coefficient $C_d = 0.61$ and fluid density $\rho = 858$ kg/m^3. The gains for the super-twisting term are selected as $\beta = 0.6$ and $\theta = 0.2$ [29]. The nonlinear coefficients γ_i chosen as $\gamma_1 = 0.33$, $\gamma_2 = 1.66$ and $\gamma_3 = 3$ to avoid the singularity condition are discussed earlier. With the parameters Θ and ζ chosen as 0.01 and 0.8, respectively, three levels of road excitation as per the ISO standard, i.e., Level A, Level B and Level C, were considered for the performance evaluation. Under the assumption that the vehicle was traveling at a fixed longitudinal speed of 40 km/h, extensive simulations were then carried out.

4.2 PSO-optimized gains and classifier training

The Off-line phase was initiated with the design of a PSO [32]-based approach to optimize the control parameter sets C_j for the proposed nonlinear feedback control (19). For every road level, each of the controllers, i.e., Controller A, Controller B and Controller C, was employed and based on the PSO the optimized parameters were computed. To apply the standard PSO technique in searching the optimal controller parameters, each particle was defined as $X = C_j = \left[\kappa_{1j}\ \kappa_{2j}\ \beta_{1j}\ \beta_{2j}\right]$. Consequently, the particles were able to automatically search for a optimal solution according to the objective function. In this work, the particle size is selected as 20 and the total number of iterations is iter $= 100$. As discussed earlier, road holding is ensured by considering the dynamic tire force constant $S_c \leq 1$ as a constraint for PSO. Based on such design, the optimized control parameters for different control sets are shown in Table 2.

Employing the generated parameters by the PSO, the performance of the proposed control was evaluated for each road class. Consequently, the above generated parameters for the controllers A, B and C as shown in Table 2 were then stored in the controller database block. With the optimized controller

Table 2 Optimized controller parameters generated by PSO

Parameter	Optimized parameters generated by PSO			
	Range	C_A	C_B	C_C
κ_1	[0, 1000]	332	440	417
κ_2	[0,1000]	365	512	990
β_1	[0, 50]	14	39	14
β_2	[0, 50]	1.7	7.8	2.6

parameters sets C_j, the classifier was then generated according to the procedure given in Sect. 3. In accordance with the objectives of choosing the insensitive index as discussed in Sect. 3, it was found that the unsprung mass acceleration measurement is invariant to the variations in the control parameter sets similar to [16]. To further illustrate this, the influence of control parameter sets on the sprung mass and unsprung mass acceleration frequency responses are shown in Fig. 5 for a Level A road. It can be seen that, in comparison with sprung mass acceleration, the unsprung mass acceleration has minimal variation under varying controller sets. Similar observations were obtained for the other levels of roads. Accordingly, considering unsprung mass accelerations as candidate response, the insensitive indexes of various road levels were computed. In this work, a classification interval of $\lambda = 1$ s was selected. The computed insensitive indexes for road levels A , B and C are shown in Fig. 6a. It can be seen from Fig. 6a that the insensitive frequency ranges for all three road levels were $aD4, aD2$ and $dA3$ with $\Omega_1 = aD4$, $\Omega_2 = aD2$ and $\Omega_3 = dA3$. With the selected insensitive frequency ranges, the statistical features databases, i.e., VAR, SRA and RMS, were computed. Consequently, the superior features were automatically selected by mRMR as RMS (time domain), SRA($aD4$), SRA ($aD2$) and SRA ($dA3$) ensuring the diversity of inputs for classifier with both the time and the frequency domain features considered. Employing these features database, the PNN classifier is then trained with the training set as shown in Table 3. To evaluate classifier performance, the F-score criterion [14] was adopted where

$$\text{F-score} = 2\frac{pr}{p+r}, \tag{41}$$

where $p = \text{RCC}/(\text{RCC} + \text{IRC})$, $r = \text{RCC}(\text{RCC} + \text{RIN})$. The classification levels are then given as RCC—

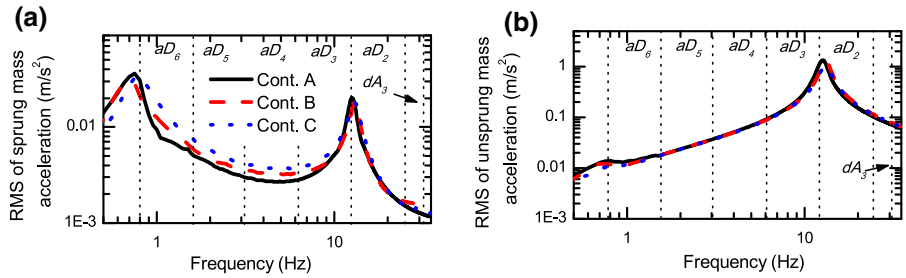

Fig. 5 Influence of controller parameters for road level A on **a** sprung mass, **b** unsprung mass

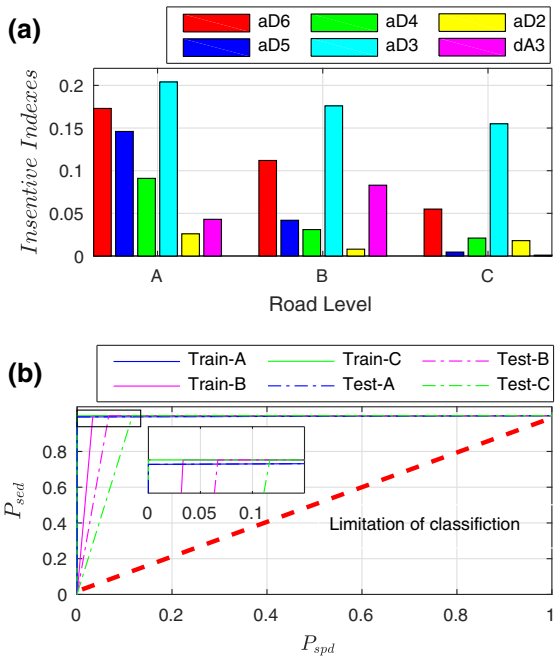

Fig. 6 **a** Computed insensitive indexes for various road levels, **b** performance of the intelligent classifier

Road Classified Correctly, IRC—Incorrect Road Classified, RIN—Road Not Identified, TN—The road is not classified due to not being present (i.e., true negative). Based on the these classification levels, the correct classification and false outputs can be defined based on the specific degree P_{spd} and the sensitivity degree P_{sed} as:

$$P_{\text{spd}} = \frac{\text{RCC}}{\text{RCC} + \text{RIN}}, P_{\text{sed}} = \frac{\text{IRC}}{\text{IRC} + \text{TN}}. \tag{42}$$

Subsequently, the receiver operating characteristic (ROC) curve showing the classification result for testing set is presented in Fig. 6b.

It can be concluded from Fig. 6b that the intelligent classifier can accurately classify road level with F-score equal to 0.987 for the testing data set. Due to the framing and overlap of 50%, no output can be obtained in the first second which leads to a RIN error. Based on the illustrated results for road classification, it can be deduced that the proposed classifier is invariant to controller parameter variations.

Table 3 Setting for training, testing and validation processes

Term	Value
Classification interval	$\lambda = 1$ s
Filter cutoff frequency	50 Hz
Overlapping	50% (100 points) for $\lambda = 1$ s
Setting of training set	150 s for each class
Sequence of training set	A, B, C Road with controller B
Setting of testing set	100 s for each class controller
Sequence of testing set	A-A,A-B,A-C,C-A,C-B,C-C
	B-A,B-B,B-C (road controller)
Setting of validation	10 s for each road level
Sequence of validation	Road level: A-B-C

4.3 On-line phase: classification-aided controller

The selection of the optimized gains of the three controllers based on PSO and the generation of the classifier for training completed the Off-line phase. Subsequently, with the validation set given in Table 3. In the On-line phase, first the unsprung mass acceleration signal with the smallest average insensitive index value (γ) is obtained and then the superior features are extracted. The road level is then identified by the trained PNN classifier. It should be noted that in the Off-line phase, the optimized control parameters w.r.t different road levels sets are stored in the controller database. Subsequently, in the On-line phase once the road level is detected, the specific controller parameter set from the controller database can be directly employed. This

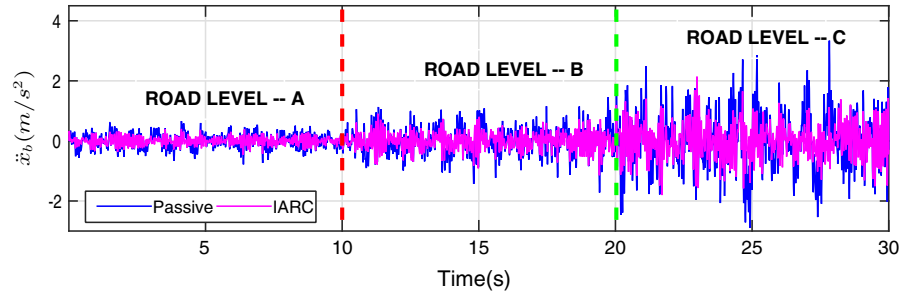

Fig. 7 Performance of the proposed RAISC over different road levels

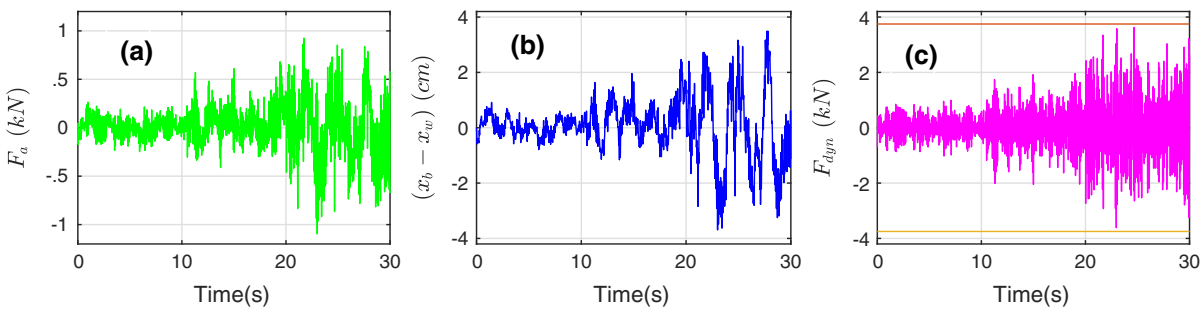

Fig. 8 System constraints **a** actuator force (F_a), **b** suspension stroke ($x_b - x_w$), **c** dynamic tire force (F_{dyn})

procedure ensures less computational time spent during the On-line phase. For the varying road conditions and controller parameters set, the proposed road classifier accurately estimated the road level with F-score equal to 0.947. Three errors appear in the first second and transition of two adjacent levels, and can be interpreted as framing and changing of dynamic response. This information of the estimated road level was then provided to the controller database block. The performance of the classification-aided controller for the road sequence as discussed in Table 3 is shown in Fig. 7.

It can be deduced from Fig. 7 that the proposed classification-aided control strategy effectively improved the passenger comfort levels in comparison with a passive system. Employing the proposed RAISC, it was found that the RMS value of sprung mass acceleration reduced by 42.9% for Level A road, by 37.8% for the Level B road and by 40.3% for the Level C road, respectively. With the reduction in sprung mass acceleration leading to increase in ride comfort, it was further ensured that the constraints on suspension stroke and actuator force along with road holding were maintained as shown in Fig. 8. Thus, the proposed RAISC control architecture for road adaptive active suspension control ensures the improvement in passenger comfort over different road conditions while maintaining road holding as shown in Fig. 8c. Further, the constraints on mechanical design and actuator limitations are also satisfied as shown in Fig. 8a, b.

5 Discussion

The effective implementation of the proposed RAISC is subject to both the classifier and the controller performance. Specifically, the influence of classification interval, selection of superior features and robustness of the controller which affect the closed-loop performance are critical.

The performance of classifier with various selected classification intervals such as 1 s, 2 s and 5 s, with 100 points from the previous frame, i.e., overlap for 66%, 50%, 33% and 16%, respectively, was detected.

It can be seen from Fig. 9a that with the increase in classification intervals the F-score value decreases. This occurs because a high value of λ slows down the adaption process and deteriorates the RAISC performance especially in complex road conditions typically for higher vehicle velocities. Similarly, if a very low classification interval, i.e., $\lambda \ll 1$ s, is selected, then very little data are available for the road classification and the performance deteriorates. Consequently,

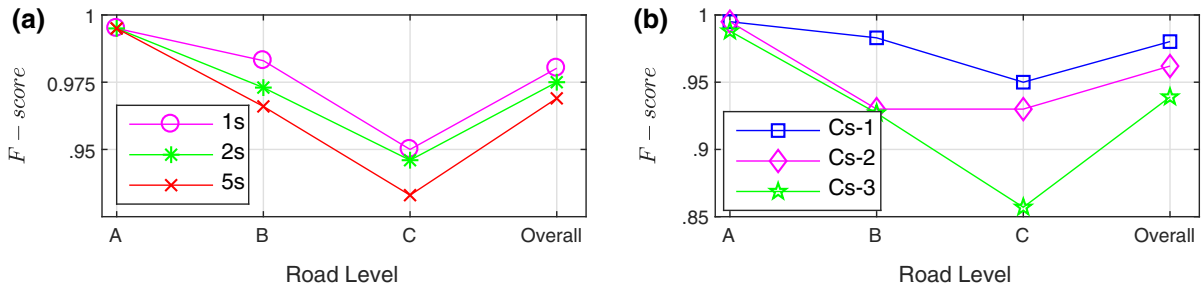

Fig. 9 F-scores showing **a** influence of classification interval, **b** effect of superior features selection

in this paper, a mid-range value $\lambda = 1$ s which has high F-score of 0.981 and satisfies the constraint (38) was selected.

The selection of superior features according to the insensitive frequency ranges θ_η also affects the performance of the classifier along with the classification interval as shown in Fig. 9b. To analyze the same, three cases were considered as: (i) Cs-1: Selection of the superior features from the time and the frequency domain while considering the insensitive frequency ranges, i.e., the proposed work, (ii) Cs-2: Selection of the features from the time and the frequency domain without considering the insensitive frequency ranges, (iii) Cs-3: Selection of the features from the time domain only without considering the insensitive frequency ranges. For both combination 1 and 2, the number of superior features are set to be 4, and candidate features number are 12 and 21 (six frequency ranges and time domain for three basic features), respectively. All of the combinations were used for PNN training with training set using the parameters given in Table 3. The comparison analysis of all three cases are presented in Fig. 9b.

It can be seen from Fig. 9b that in the cases where insensitive frequencies are considered for selection of superior features, the classification performance is high. Further, for worsening road levels, i.e., B and C, it can be seen that the proposed method outperforms both the cases where features from time and frequency domain without considering insensitive frequency ranges were considered and when only features from time domain were considered. It can be hence deduced that for the nonlinear suspension system with varying active control provided, the selection of superior features considering the insensitive frequency ranges from both the time and the frequency domain generates the best result.

Table 4 Reduction in RMS of sprung mass acceleration

Roads	Passive	ANN	IHOSM	RAISC
A	0.233	0.175 (25%)	0.147 (37%)	0.133 (43%)
B	0.444	0.337 (24%)	0.306 (31%)	0.276 (38%)
C	0.933	0.668 (28%)	0.595 (36%)	0.557 (40%)
All	0.611	0.445 (27%)	0.401 (34%)	0.396 (40%)

The closed-loop performance of the proposed classification-aided controller is also affected by selection of the control gains. To select optimal gains, PSO technique was employed in this paper as discussed in Sect. 4.2. The percentage improvement in ride comfort indicated by the decrease in sprung mass acceleration when the controllers designed above were employed to the three road levels is shown in Table 4. To compute the percentage decrease in sprung mass acceleration, the following expression was used:

$$\%\,\text{Decrease} = 1-(\text{RMS}(\ddot{x}_b)_{\text{active}})/((\text{RMS}(\ddot{x}_b)_{\text{passive}})). \tag{43}$$

It can be seen from Table 4 that in comparison with a passive system, a backstepping-based controller based on IHOSM [22] and an ANN-based controller [10], the proposed RAISC design leads to better improvement in ride comfort by the decrease in sprung mass acceleration. It is of note that to ensure the optimal gains for the controllers, PSO was employed for all three designs, i.e., I-HOSM, ANN controller and the proposed RAISC design. The RAISC controller outperforms the other controllers in each road level and also for the entire testing sequence. For the suspension system, the frequency domain ride performance is often evaluated by the computing the PSD of the sprung mass acceleration [4,33]. Accordingly, the performance of the proposed

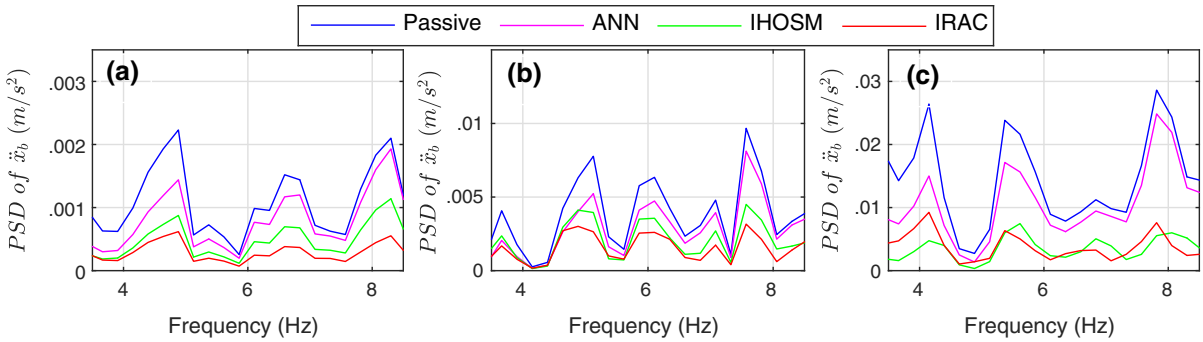

Fig. 10 PSD of sprung mass acceleration compared for **a** Level A, **b** Level B, **c** Level C roads

Table 5 RMS of sprung mass acceleration in the presence of noise and uncertainty using RAISC

Type	Conditions		% Decrease RMS $\ddot{x}_b$		
	Parameter	Uncertainty	A	B	C
Uncertainty	m_b	5%	40.3	34.1	37.3
		7.5%	38.1	31.9	35.5
	k_s	10%	38.9	37.1	35.8
		20%	34.3	32.3	30.5
	c_p	10%	37.7	32.6	30.5
		20%	32.2	27.7	25.8
	β_e, C_{tp}	5%	37.7	32.9	31.5
		7.5%	34.7	29.9	28.2
Sensor noise	$x_b - x_w$	25×10^{-4}	39.1	33.1	35.1
		5×10^{-3}	38.2	32.2	30.7

RAISC design in compassion with the other controllers is shown in Fig. 10 for road levels A, B and C. It can be seen that for the considered frequency range, the proposed design has better performance than the other controllers.

The performance of RASIC in the presence of sensor noise and parametric uncertainties was also analyzed for robustness analysis. For the suspension system, various parameters such as spring stiffness, leakage coefficient of actuator and bulk modulus of liquid used exhibit uncertain behavior [4,23] with temperature variations and component condition deterioration. The performance of RAISC in the presence of different levels of uncertainties in the suspension, hydraulic actuator parameters and sensor noise is shown in Table 5.

As shown in Table 5, for different levels of parameter uncertainty in sprung mass, spring stiffness, damping, effective bulk modulus and piston leakage coefficient, the percentage reduction in sprung mass acceleration is in the range of 30–40%. Particularly, it can be seen that even for a Class C road, with parametric uncertainty in suspension damping up to 20%, the reduction in sprung mass acceleration remains fairly good. Similar results can be seen for various parametric uncertainties over road levels A, B and C. Further, the results with the presence of sensor noise in the suspension stroke, considered as measured output for the controller design also exhibits good reduction in sprung mass acceleration. This implies that passenger comfort is duly enhanced for the uncertain suspension system. Based on the results shown in Table 5, the robust performance of the proposed RAISC approach under uncertain parametric behavior and sensor noise can be established.

However, the approach is subject to some limitations such as the selection of a reference tracking and effect of varying control strategies. Thus, when the control strategy is changed, the whole procedure aforementioned should be performed again to formulate a

new classifier. This is, however, a general limitation of data-driven-based road classification methods with the specific control objectives. During the course of performance evaluations, it was considered that $x_d = 0$ similar to the work in [4,8]. This is generally considered because the suspension stroke tracking is not generally quantified as a measure of the suspension performance. Having said that in [23], a polynomial reference signal based on the time of convergence was proposed. However, this approach was applied to track the sprung mass displacement and has not been employed for the suspension stroke signal. Based on above conclusions, we have considered zero reference even when the road disturbance is random in nature and the performance is shown. In future work, we would look to develop/propose a reference signal based on performance criteria suited for random roads similar to works of [23,34].

6 Conclusion

In this work, an intelligent robust state feedback control approach was proposed for the active control of a nonlinear suspension system equipped with hydraulic actuators and by varying road disturbance levels as per ISO standards. Initially, the control was formulated using the robust higher-order terminal sliding mode approach and the control parameters for each road level were optimized using PSO. Subsequently, a novel classification approach which is invariant to the control parameter variations was proposed to identify the road levels in real time. Integrating the information classified road levels and the optimized control parameters, the nonlinear control was implemented for a sequence of varying road levels. Simulation scenarios presented show the efficiency of the proposed intelligent controller in comparison with other control approaches for improvement in the ride comfort. Extensive discussions were provided detailing the influence of classification interval and features selection to show the efficiency of the proposed scheme.

Acknowledgements The authors acknowledge the support of the National Natural Science Foundation of China (Grant No. 51805028) and China Postdoctoral Science Foundation (Grant Nos. 2016M600934, BX201600017).

References

1. Sun, W., Gao, H., Yao, B.: Adaptive robust vibration control of full-car active suspensions with electrohydraulic actuators. IEEE Trans. Control Syst. Technol. **21**(6), 2417–2422 (2013)
2. Zirkohi, M., Lin, T.: Interval type-2 fuzzy-neural network indirect adaptive sliding mode control for an active suspension system. Nonlinear Dyn. **79**(1), 513–526 (2015)
3. Jones, W.D.: Easy ride: Bose Corporation uses speaker technology to give cars adaptive suspension. IEEE Spectr. **42**(5), 12–14 (2005)
4. Rath, J.J., Defoort, M., Veluvolu, K.C., Karimi, H.R.: Output feedback active suspension control with higher order terminal sliding mode. IEEE Trans. Ind. Electron. **64**(2), 1392–1403 (2016)
5. Kilicaslan, S.: Control of active suspension system considering nonlinear actuator dynamics. Nonlinear Dyn. **91**(2), 1383–1394 (2018)
6. Tseng, H.E., Hrovat, D.: State of the art survey: active and semi-active suspension control. Veh. Syst. Dyn. **53**(7), 1034–1062 (2015)
7. Xiao, L., Zhu, Y.: Sliding-mode output feedback control for active suspension with nonlinear actuator dynamics. J. Vib. Control **20**(9), 1–18 (2013)
8. Li, H., Jing, X., Karimi, H.: Output feedback based H-infinity control for vehicle suspension systems with control delay. IEEE Trans. Ind. Electron. **61**(1), 436–446 (2014)
9. Yin, S., Huang, Z.: Performance monitoring for vehicle suspension system via fuzzy positivistic C-means clustering based on accelerometer measurements. IEEE/ASME Trans. Mechatron. **20**(5), 2613–2620 (2015)
10. Zhao, F., Ge, S.S., Tu, F., Qin, Y., Dong, M.: Adaptive neural network control for active suspension system with actuator saturation. IET Control Theory Appl. **10**(14), 1696–1705 (2016)
11. Qin, Y., Langari, R., Wang, Z., Xiang, C.: Road excitation classification for semi-active suspension system with deep neural networks. J. Intell. Fuzzy Syst. **33**(3), 1907–1918 (2017)
12. Qin, Y., Langari, R., Wang, Z., Xiang, C.: Road profile estimation for semi-active suspension using an adaptive Kalman filter and an adaptive super-twisting observer. In: IEEE Proceedings of American Control Conference, pp. 973–978 (2017)
13. Tudon-Martinez, J. C., Fergani, S., Varrier, S., Sename, O., Dugard, L., Morales-Mendez, R., Ramirez-Mendoza, R.: Road adaptive semi-active suspension in an automotive vehicle using an LPV controller. In: Proceedings of 7th IFAC Symposium on Advances in Automotive Control, pp. 231–236 (2013)
14. Tudon-Martinez, J.C., Fergani, S., Varrier, S., Sename, O., Martinez, J.J., Morales-Mendez, R., Dugard, L.: Adaptive road profile estimation in semiactive car suspensions. IEEE Trans. Control Syst. Technol. **23**(6), 2293–2305 (2015)
15. Formentin, S., Karimi, A.: A data-driven approach to mixed-sensitivity control with application to an active suspension system. IEEE Trans. Ind. Inform. **9**(4), 2293–2300 (2013)

16. Qin, Y., Xiang, C.L., Wang, Z., Dong, M.: Road excitation classification for semi-active suspension system based on system response. J. Vib. Control **24**(13), 2732–2748 (2019)
17. Qin, Y., Dong, M., Zhao, F., Langari, R., Gu, L.: Road profile classification for vehicle semi-active suspension system based on adaptive neuro-fuzzy inference system. In: Proceeding of IEEE Control Decision Conference (CDC), pp. 1533–1538 (2015)
18. Fialho, I., Balas, G.J.: Road adaptive active suspension design using linear parameter-varying gain-scheduling. IEEE Trans. Control Syst. Technol. **10**(1), 43–54 (2002)
19. Kanarachos, S., Kanarachos, A.: Intelligent road adaptive suspension system design using an expertsbased hybrid genetic algorithm. Expert Syst. Appl. **42**(21), 8232–8242 (2015)
20. Huang, C.J., Lin, J.S., Chen, C.C.: Road-adaptive algorithm design of half-car active suspension system. Expert Syst. Appl. **37**(6), 4392–4402 (2010)
21. Gohrle, C., Schindler, A., Wagner, A., Sawodny, O.: Road profile estimation and preview control for low-bandwidth active suspension systems. IEEE/ASME Trans. Mechatron. **20**(5), 2299–2310 (2015)
22. Defoort, M., Floquet, T., Kokosy, A., Perruquetti, W.: A novel higher order sliding mode control scheme. Syst. Control Lett. **58**(2), 102–108 (2009)
23. Sun, W., Gao, H., Kayanak, O.: Adaptive backstepping control for active suspension systems with hard constraints. IEEE/ASME Trans. Mechatron. **18**(3), 1072–1079 (2012)
24. ISO.: Mechanical vibration–road surface profiles–reporting of measured data. ISO 8608 (1995)
25. Yao, J., Jiao, Z., Ma, D.: Extended-state-observer-based output feedback nonlinear robust control of hydraulic systems with backstepping. IEEE Trans. Ind. Electron. **61**(11), 6285–6293 (2014)
26. Hu, C., Wang, R., Yan, F.: Integral sliding mode-based composite nonlinear feedback control for path following of four-wheel independently actuated autonomous vehicles. IEEE Trans. Transp. Electr. **2**(2), 221–230 (2016)
27. Hu, C., Wang, R., Yan, F.: Differential steering based yaw stabilization using ISMC for independently actuated electric vehicles. IEEE Trans. Intell. Transp. Syst. **19**(2), 627–638 (2018)
28. Chiu, C.S.: Derivative and integral terminal sliding mode control for a class of MIMO nonlinear systems. Automatica **48**(2), 316–326 (2012)
29. Chen, Y., Dong, H., Lv, J.: A super-twisting-like algorithm and its application to train operation control with optimal utilization of adhesion force. IEEE Trans. Intell. Transp. Syst. **17**(11), 3035–3044 (2016)
30. Bacciotti, A., Rosier, L.: Liapunov Functions and Stability in Control Theory. Springer, Berlin (2006)
31. Specht, D.: Probabilistic neural networks. Neural Netw. **3**(1), 109–118 (1990)
32. Poli, R., Kennedy, J., Blackwell, T.: Particle swarm optimization. Swarm Intell. **1**(1), 33–57 (2007)
33. Poussot-Vassal, C., Spelta, C., Sename, O., Savaresi, S., Dugard, L.: Survey on some automotive semi-active suspension control methods: a comparative study on a single-corner model. In: 18th IFAC World Congress, Milan, Italy, pp. 1802–1807 (2011)
34. Wang, G., Chen, C., Yu, S.: Finite time sliding mode tracking control for active suspension systems via extended super-twisting observer. Proc. Inst. Mech. Eng. Part 1 J. Syst. Control Eng. **231**(6), 1–6 (2017)